

On Beaming Effects in Afterglow Light Curves

R. Moderski^{1,2,3}, M. Sikora^{2,3}, and T. Bulik²

¹ JILA, University of Colorado, Boulder

² Nicolaus Copernicus Astronomical Center, Warsaw

³ ITP, University of California, Santa Barbara

Received _____; accepted _____

ABSTRACT

The most luminous GRBs can be explained in terms of models involving stellar mass central engines only if the ejecta are beamed. As was pointed out by Rhoads (1997), the dynamics of the blast wave, formed by the beamed ejecta sweeping the external gas, can be significantly modified by the sideways expansion. This is because in this case the surface of the blast wave increases faster than just due to the radial divergence and so the blast wave deceleration rate increases faster. According to analytical estimates, the effect becomes important shortly after the bulk Lorentz factor of the blast wave drops below the inverse of the initial opening angle of the beamed ejecta and is accompanied by a sharp break in the afterglow light curve.

However, our numerical studies, which follow the dynamical evolution of the blast wave, the evolution of the electron energy distribution, and take into account the light travel effects related to the lateral size of the source, show that the break of the light curve is weaker and much smoother than the one analytically predicted. A prominent break emerges only for a model without sideways expansion.

Subject headings: gamma rays: bursts

1. INTRODUCTION

Beaming of relativistic ejecta in GRBs has been postulated by many authors in order to ease the GRB energy budget (see, *e.g.*, Mészáros, Rees, & Wijers 1998 and refs. therein). There are basically two ways to verify the beaming observationally: one is statistical and is based on counting the afterglow like transient sources and comparing their rate with the GRB rate, and the second one is related to the beaming effects predicted to be imprinted in the afterglow light curves of individual objects (Rhoads 1997). Applying the first method to the X-ray transient sources, Grindlay (1999) found that results are consistent with no beaming differentiating the GRB and X-transient rates. However, as was pointed out by Woods & Loeb (1999), the conclusive results about excess (or its lack) of X-ray transients over GRBs must wait for much more sensitive future instruments. This is because statistically significant contribution to the excess of X-ray transients over GRBs is expected to be provided only by weak X-ray transients, those representing afterglows phases when the bulk Lorentz factor of the radiating shell drops below the inverse of its angular size. Similar studies can be performed also in optical and radio band (Rhoads 1997; Woods & Loeb 1999).

In individual objects, the beaming related effects are expected to be imprinted in the optical and X-ray afterglow light-curves. The lateral expansion of the shocked, relativistic plasma causes that at some moment the front of the blast wave starts to increase faster than due to the cone-outflow (Rhoads 1997). Due to this the blast wave begins to decelerate faster than without the sideways outflows and this produces a break in the light curve, the sooner the larger the beaming factor is. Such a break is claimed to be present in the light curve of GRB 990123, the most energetic GRB up to date (Kulkarni *et al.* 1999). Sari, Piran, & Halpern (1999) speculate that afterglows with very steep light curves are highly beamed. Possibly the break in such objects is not recorded because it took place before the

optical follow-ups.

As now, all theoretical studies of the light-curve breaks are analytical and are based on: power-law approximation of the blast wave dynamics, broken power-law approximation of radiation spectra and on “on-axis” relation between the observed flux and the emitted flux (Rhoads 1977, 1999; Kulkarni *et al.* 1999; Sari, Piran, & Halpern 1999). In this paper, we treat the dynamics using the prescription given by Blandford and McKee (1976). The evolution of radiation spectrum is calculated exactly, by computing the time evolution of electrons from continuity equation and by computing the observed luminosity through integrating the emitted radiation over the “ $t = \text{const}$ ” surfaces. Our results show that the change of the light curve slope is significant, but smaller than predicted analytically. And, what is more important, the light curves steepen very slowly, so that it is very difficult to talk about the specific time location of the break. In order to demonstrate better the beaming effect, we compare our results with the spherical case. We also show how the light curve should look like if there is no lateral expansion.

In §2 we collect equations, which are used to compute the blast wave speed, evolution of electrons, and afterglow light-curves. In §3 we present results of our numerical studies of afterglows produced by beamed ejecta, and, in §4 we compare them with simple analytical estimations.

2. BASIC EQUATIONS

2.1. Dynamics

The deceleration of a blast wave is described by the following equations (Blandford & McKee 1976; Chiang & Dermer 1998):

$$\frac{d\Gamma}{dm} = -\frac{\Gamma^2 - 1}{M}, \quad (1)$$

$$\frac{dM}{dr} = \frac{dm}{dr} [\Gamma - \epsilon_{rad} \epsilon_e (\Gamma - 1)], \quad (2)$$

and

$$dm/dr = \Omega_j r^2 \rho = 2\pi r^2 (1 - \cos\theta_j) \rho, \quad (3)$$

where Γ is the bulk Lorentz factor of the blast wave, M is the total mass including internal energy, r is the distance from the central engine to the blast wave, dm is the rest mass swept up in the distance dr , ρ is the mass density of the external medium, ϵ_e is the fraction of dissipated energy converted to relativistic electrons, ϵ_{rad} is the fraction of electron energy which is radiated, and θ_j is the angular size of the blast wave. This angular size is not constant but increases due to thermal expansion (Rhoads 1997),

$$\theta_j \equiv \frac{a}{r} = \theta_{j0} + \frac{v'_l}{c\Gamma}, \quad (4)$$

where the speed of the lateral expansion, v'_l , is assumed by Rhoads (1999) to be equal to the sound speed in the relativistic plasma, $c_s = c/\sqrt{3}$, but considered by Sari *et al.* (1999) to be relativistic. Noting, that the plasma in the blast wave is continuously loaded by the fresh gas which initially doesn't have any lateral bulk speed, one can expect that in reality v'_l does not reach relativistic value and sets up somewhere between c_s and $\beta_\Gamma c$, and in general depends on r , and on θ_j .

2.2. Electron energy distribution

We assume that the electrons are injected with the power law energy distribution

$$Q = K\gamma^{-p}, \quad (5)$$

with the minimum energy of injected electrons

$$\gamma_m = \frac{\epsilon_e (\Gamma - 1) m_p}{m_e} \frac{p - 2}{p - 1}. \quad (6)$$

The maximum energy of injected electrons for a given magnetic field, B' , is assumed to be given by (de Jager *et al.* 1996):

$$\gamma_{max} \simeq 4 \times 10^7 \left(\frac{B'}{1\text{G}} \right)^{-1/2} \quad (7)$$

Normalization of the injection function, K , is provided by

$$L'_{e,inj} \equiv \int_{\gamma_m}^{\gamma_{max}} Q \gamma m_e c^2 d\gamma = \epsilon_e \frac{dE'_{acc}}{dt'}, \quad (8)$$

where

$$\frac{dE'_{acc}}{dt'} = \frac{dr}{dt'} \frac{dE'_{acc}}{dr} = \frac{dr}{dt'} \frac{dm}{dr} c^2 (\Gamma - 1) = \Omega_j r^2 \rho \beta_\Gamma \Gamma (\Gamma - 1) c^3, \quad (9)$$

is the rate of accreted kinetic energy, $dr = c \beta_\Gamma \Gamma dt'$, $\beta_\Gamma = \sqrt{\Gamma^2 - 1}/\Gamma$, and t' is the time measured in the blast wave comoving frame.

The evolution of the electron energy distribution is given by the continuity equation

$$\frac{\partial N_\gamma}{\partial r} = \frac{\partial}{\partial \gamma} \left(N_\gamma \frac{d\gamma}{dr} \right) + Q, \quad (10)$$

where

$$\frac{d\gamma}{dr} = -f(r) \gamma^2 - g \frac{\gamma}{r}, \quad (11)$$

are the electron energy losses. In both equations above, the derivatives over comoving time t' have been replaced by the derivatives over the distance r , according to the relation $\partial/\partial t' = c \beta_\Gamma \Gamma \partial/\partial r$. The first term on the rhs of Eq. (11) represents synchrotron plus Compton energy losses, *i.e.*,

$$f(r) = \frac{\sigma_T}{6m_e c^2} \frac{B'^2}{\beta_\Gamma \Gamma} (1 + u'_s/u'_B), \quad (12)$$

where $u'_B = B'^2/8\pi$ is the magnetic energy density, and u'_s is the energy density of the synchrotron radiation, both as measured in the blast wave frame. The second term on the rhs of Eq. (11) represents the adiabatic losses. The parameter g depends on the geometry

of the expansion; for 2-dimensional (lateral) expansion $g = 2/3$, and for 3-dimensional expansion $g = 1$.

We calculate the magnetic field following Chiang & Dermer (1999)

$$u'_B \equiv \frac{B'^2}{8\pi} = \epsilon_B \kappa \rho c^2 \Gamma^2, \quad (13)$$

where κ is the compression ratio and ϵ_B parameterizes the departure of the magnetic field intensity from its equipartition value.

2.3. Synchrotron spectrum

The evolution of the synchrotron spectrum in the blast wave frame is given by

$$L'_{syn,\nu'}(r) = \int N_\gamma(r) P(\nu', \gamma) d\gamma, \quad (14)$$

where $P(\nu', \gamma)$ is the power spectrum of synchrotron radiation of a single electron in isotropic magnetic field (see, *e.g.*, Chiaberge & Ghisellini 1999).

The apparent monochromatic synchrotron luminosity as a function of time (a light curve) is calculated from

$$L_{syn,\nu}(t, \theta_{obs}) = \iint_{\Omega_j} \frac{L'_{syn,\nu'}[r(\tilde{\theta})] \mathcal{D}^3}{\Omega_j} d \cos \tilde{\theta} d\tilde{\phi}, \quad (15)$$

where $\mathcal{D} = 1/\Gamma(1 - \beta_\Gamma \cos \tilde{\theta})$ is the Doppler factor of the blast wave at the angle $\tilde{\theta}$. The coordinates $(\tilde{\theta}, \tilde{\phi})$ are chosen so that the observer is located at $\tilde{\theta} = 0$ ($\theta = \theta_{obs}$) and the jet axis is at $\tilde{\theta} = \theta_{obs}$. The integral is taken over the surfaces

$$t = \int \frac{(1 - \beta_\Gamma \cos \tilde{\theta})}{c\beta_\Gamma} dr = \text{const}, \quad (16)$$

enclosed within the blast wave boundaries, Ω_j .

2.4. Inverse-Compton radiation

We assume hereafter that cooling of relativistic electrons is dominated by synchrotron radiation, *i.e.* that $u'_s \ll u'_B$. This condition will be verified and discussed in Appendix A.

3. RESULTS

We have used the following model parameters of the afterglow model in our calculations: initial energy per solid angle, $E_0/\Omega_{j0} = 10^{54} \text{ ergs s}^{-1}/4\pi$; $\Gamma_0 = 300$; $\theta_{j0} = 0.2$; $\kappa = 4$; $\rho = m_p/1\text{cm}^3$; $\epsilon_e = 0.1$ (the quasi-adiabatic case); $\epsilon_B = 0.03$; $p = 2.4$. The parameters were not chosen to fit any specific observations, but rather to demonstrate the difference between simple analytical predictions and self-consistent numerical calculations regarding the beaming effects in a light-curves.

In Fig. 1 we present the dependence of a bulk Lorentz factor of the blast wave on its distance from the central engine. We show three solutions for three different values of v'_l : $v'_l = 0$ (thin line); $v'_l = c/\sqrt{3}$ (solid line); and $v'_l = c$ (dotted line). For $v'_l = 0$ ($\rightarrow \theta_j = \text{const}$) and $r_0 \ll r \ll r_{nr}$, the bulk Lorentz factor is well approximated by

$$\Gamma \simeq \Gamma_0 (r_0/r)^{3/2}, \quad (17)$$

where

$$r_0 \simeq \left(\frac{3E_0}{\Gamma_0^2 \rho c^2 \Omega_j} \right)^{1/3} \simeq 1.2 \times 10^{17} \text{ cm}, \quad (18)$$

is the radius where deceleration of the GRB ejecta by sweeping of interstellar gas starts to be efficient, and

$$r_{nr} \simeq r_0 \left(\frac{\Gamma_0}{2} \right)^{2/3} \simeq 3.4 \times 10^{18} \text{ cm}, \quad (19)$$

is the radius above which the blast wave becomes nonrelativistic. Fig. 1 demonstrates that steepening of the $\Gamma(r)$ curves due to lateral outflow is very smooth, without any sharp

break like the one predicted analytically to take place at a distance, at which Γ drops below $1/\theta_{j0}$, *i.e.* at

$$r_D \simeq r_0(\Gamma_0\theta_{j0})^{2/3} \simeq 1.8 \times 10^{18} \text{cm}. \quad (20)$$

In Fig. 2 we show the radial dependence of the rate of kinetic energy accreted by the blast wave, dE'_{acc}/dt' (see Eq. 9). As one could expect, the larger the lateral outflow speed, the larger the accretion rate is. The steepening of curves at large r is due to transition from the relativistic regime ($\Gamma > 2$) to the nonrelativistic regime, where dE'_{acc}/dt' is significantly reduced, and becomes $\propto (\Gamma - 1)$ (see Eq. 9). When divided by ϵ_e , curves in Fig. 2 illustrate also the r dependence of injection luminosity of relativistic electrons (see Eq. 8).

In Fig. 3 we show time evolution of the electron energy distribution, N_γ , multiplied by γ^2 . The curves are calculated at such values of the radius r , from which the signal produced on the axis $\tilde{\theta} = 0$ is reached by the observer $t = 1, 10, 10^2, \dots, 10^7$ seconds after “the signal” from $r = 0$. The relation between r and t is

$$t = \int_0^r \frac{(1 - \beta_\Gamma)}{c\beta_\Gamma} dr \simeq \int_0^r \frac{1}{2c\Gamma^2} dr. \quad (21)$$

The peak positions of the $N_\gamma\gamma^2$ curves mark Lorentz factor of those electrons which carry most of leptonic energy at a given distance. For injection spectral index $2 < p < 3$, the peak is located at γ_m given by Eq. (6), and this is the case in our model. Another characteristic energy is

$$\gamma_c = 6.1 \times 10^{20} \frac{m_p}{\epsilon_B \kappa \rho r \Gamma}, \quad (22)$$

below which the time scale of electron energy losses due to synchrotron radiation is longer than the dynamical time scale. We present the dependence of γ_m and γ_c on the radius r in Fig. 4.

We can see from Fig. 4, that for the first 5 curves presented in the Fig. 3, $\gamma_m > \gamma_c$. In this case, in accordance with the analytical predictions, the electron spectra at $\gamma > \gamma_m$

are well described by the power-law function, $N_\gamma \propto \gamma^{-s}$, with the index $s = p + 1$. For $\gamma_c < \gamma < \gamma_m$, analytical crude estimations predict $s = 2$, which in our plot should be represented by horizontal lines. This, however, is expected to be true only for $\gamma_c \ll \gamma < \gamma_m$. In our model the ratio γ_m/γ_c is not large enough to provide space for $s = 2$ and there is a smooth transition to very hard low energy tail reached by electrons due to adiabatic losses. For $\gamma_c > \gamma_m$, which is the case for the top 4 curves in the Fig. 3, the predicted electron spectra should have a slope $s = p + 1$ for $\gamma > \gamma_c$, and $s = p$ for $\gamma_m < \gamma < \gamma_c$. The former is seen, but the latter, again, due to narrow range between γ_c and γ_m doesn't apply. Instead, there the log-energy distribution is curved, smoothly joining the high energy portion of the electron spectrum with its low energy adiabatic part. Let us note, that very steep low energy tails of the curves on top of the plot result from the fact that there is not enough time for electrons to drift adiabatically to lower energies. Note also, that the details of the low energy parts of the electron energy distribution are not important, because contribution of electrons from these parts to the observed radiation is negligible.

In Fig. 5 we present the observed radiation spectra computed for the same sequence of t , as electron energy distributions shown in Fig. 3. It should be pointed out, however, that unlike in simple analytical calculations, they are computed by integration of electron radiation from $t = \text{const}$ surfaces (see Eq. 16), *i.e.* taking into account light travel differences between photons emitted at different $\tilde{\theta}$'s. The observed radiation spectra are peaked around $h\nu \sim \Gamma\gamma_m^2 B/B_{cr} m_e c^2$, where rhs quantities are calculated for r given by Eq. (16) and $B_{cr} = 2\pi m_e^2 c^3 / h e \simeq 4.4 \times 10^{13}$ Gauss. As we can see from Fig. 5, the high energy and the low energy parts of the observed radiation spectra are well described by power-law functions $L_\nu \propto \nu^{-\alpha}$, with $\alpha = p/2 = 1.1$ and $\alpha = -1/3$, respectively. The former is produced, as predicted analytically, by electrons with $\gamma > \text{Max}[\gamma_m; \gamma_c]$, the latter represents the low energy synchrotron radiation of electrons with energies $\gamma < \text{Min}[\gamma_c; \gamma_m]$. These high and low energy spectrum portions are joined very smoothly without showing any intermediate

piece of the power-law spectrum. This smoothing of the observed radiation spectra results mainly from the fact that the observed radiation at any given moment is contributed by radiation from $t = \text{const}$ surfaces, *i.e.* from different radii.

The light curves, computed for $\nu = 4.2 \times 10^{14}\text{Hz}$ and $\nu = 2.5 \times 10^{17}\text{Hz}$, are shown in Fig. 6. In this calculation we used $v'_l = c/\sqrt{3}$ and considered two different locations of the observer, $\tilde{\theta} = 0$ and $\tilde{\theta} = 0.28$. The latter case is for the observer located outside the initial ejecta cone.

In order to demonstrate better the beaming effect and its dependence on v'_l , we plot in Fig. 7 four optical light curves; three for different values of v'_l : 0, $c/\sqrt{3}$, and c , and the fourth one for the spherical outburst. We can see, that for models with lateral expansion the steepening of the light curves is extended over more than two time decades and, down to nonrelativistic regime, doesn't reach analytically predicted slope $\beta = p$ ($L_\nu \propto t^{-\beta}$). Sharp break is found only for $v'_l = 0$ model, and, it emerges shortly after $t(r_D)$, as theoretically predicted.

We should note here, that our calculations of the model with the outflows expansion are not fully consistent, because the Doppler factor includes only the radial component of the bulk motion. This, however, is expected to affect only the results of the $v_l = c$ model, where we overestimate the radiation contributed from the blast wave edge.

4. DISCUSSION AND CONCLUSIONS

The afterglows provide exceptional opportunity to study whether and how much the GRB ejecta are beamed. As predicted by Rhoads (1997), the beamed outflows should diverge from the cone geometry while decelerated by sweeping up the external gas. The sideways outflow of the shocked relativistic plasma increases the front of the blast wave

leading to a faster deceleration. Rhoads (1997) showed, using simple analytical analyses, that this should be imprinted in the light curve as a break around $t(r_D)$, *i.e.* when Γ drops below $(c_l/c)/\theta$. There the light curve should steepen, changing the slope from $\beta = (3p - 2)/4$ (for $\gamma > \text{Max}[\gamma_c; \gamma_m]$) or from $\beta = 3(p - 1)/4$ (for $\gamma_m < \gamma < \gamma_c$) (Sari, Piran, & Narayan 1998) to $\beta = p$ (Rhoads 1999). Our numerical results agree only qualitatively with these predictions. The steepening does occur, however, the slope change is smaller (to about 2.0 instead of $p = 2.4$) and is extended over more than two decades of the observed time.

There are two reasons why, contrary to simple analytical estimations, the distinct break does not emerge in our calculations. First, as is shown in Fig. 1, the dynamics of the blast wave is affected by the lateral outflow very smoothly over the whole deceleration phase, and not just around r_D (note, that at r_D the blast wave area is already almost 4 times larger than it would be without the sideways expansion). Second, the observed radiation at any given moment t is contributed by the plasma which at larger θ emits radiation from smaller r , and noting, that at smaller r plasma is moving faster and radiating stronger than at larger r , the contribution of the off-axis plasma to the observed radiation is larger than in the case of radiation contribution taken from $r = \text{const}$ surfaces as calculated analytically.

The steepening of the light curve is predicted also for the beamed ejecta without the lateral outflows. In this case, because no change of dynamics and small light travel effects at $r > r_b$ (note that there the Doppler cone becomes narrower than the ejecta cone), the break is very well located, just around the time the Γ drops below $1/\theta_j$, and the light curve steepens by $\Delta\beta = 3/4$, in accordance with analytical predictions (see, *e.g.*, Mészáros & Rees 1999).

It should be emphasized, however, that our treatment of the dynamics with the sideways expansion is based on the approximation, that at any r the material is uniformly

distributed across the blast wave. In reality, the lateral outflow can create θ dependent structure, with the density of the swept material and the radial bulk Lorentz factor decreasing sideways, and in this case the break in the light curve may become more prominent. 2D-hydro relativistic simulations are required to verify this.

This project was partially supported by NSF grant No. AST-9529175, ITP/NSF grant No. PHY94-07194, and the Polish KBN grant No. 2P03D 00415. MS and RM thank Fellows of ITP/UCSB for hospitality during the visit and participating in the program “Black Hole Astrophysics”. RM thanks NASA for support under the Long Term Space Astrophysics grant NASA-NAG-6337. MS acknowledges financial support of NASA/RXTE and ASTRO-E observing grants to USRA (G. Madejski, PI).

REFERENCES

- Blandford, R.D., & McKee, C.F. 1976, *Phys. Fluids*, 19, 1130
- Chiaberge, M., & Ghisellini, G., 1998, astro-ph/9810263
- Chiang, J., & Dermer, C.D. 1998, astro-ph/9803339
- Grindlay, J.E. 1999, *ApJ*, 510, 710
- de Jager, O.C., *et al.* 1996, *ApJ*, 457, 253
- Kulkarni, S.R. *et al.* 1999, astro-ph/9902272
- Mészáros, P., & Rees, M.J. 1999, astro-ph/9902367
- Mészáros, P., Rees, M.J., & Wijers, R.A.M.J. 1999, astro-ph/9808106
- Rhoads, J.E. 1997, *ApJ*, 487, L1
- Rhoads, J.E. 1999, astro-ph/9903399
- Sari, R., Piran, T., & Narayan, R. 1998, *ApJ*, 497, L17
- Sari, R., Piran, T., & Halpern, J.P. 1999, astro-ph/9903339
- Woods, E., & Loeb, A. 1999, astro-ph/9903377

A. INVERSE COMPTON COOLING

The ratio of inverse Compton luminosity to synchrotron luminosity is given by

$$\frac{L'_C}{L'_s} = \frac{u'_s}{u'_B}, \quad (\text{A1})$$

where

$$u'_s \simeq \frac{L'_s}{2c\Omega_j r^2}, \quad (\text{A2})$$

$$L'_s = (1 - \eta_C)\epsilon_{rad}\epsilon_e \frac{dE'_{acc}}{dt'}, \quad (\text{A3})$$

dE'_{acc}/dt' and u'_B are given by Eq. (9) and (13), respectively, and $\eta_C = L'_C/(L'_C + L'_s)$. Using all these relations in Eq. (A1), we find that for $\Gamma \gg 1$

$$\frac{L'_C}{L'_s} = \frac{(1 - \eta_C)\epsilon_{rad}\epsilon_e}{2\kappa\epsilon_B}, \quad (\text{A4})$$

and noting that $L'_C/L'_s = \eta_C/(1 - \eta_C)$, we obtain

$$\eta_C = \frac{(1 + 2\chi) - \sqrt{1 + 4\chi}}{2\chi}, \quad (\text{A5})$$

where

$$\chi = \frac{\epsilon_{rad}\epsilon_e}{2\epsilon_B\kappa}. \quad (\text{A6})$$

and for $\chi \ll 1$, $\eta_C \simeq \chi$.

For $\gamma_m > \gamma_c$ practically all energy converted to electrons is radiated ($\epsilon_{rad} \simeq 1$) and the inverse Compton is energetically negligible ($\eta_C \ll 1/2$) if $\epsilon_B > 10^{-2}$. For $\gamma_m < \gamma_c$, the luminosity peaks at ν_c and

$$\epsilon_{rad} \simeq \left(\frac{\gamma_m}{\gamma_c}\right)^{p-2}. \quad (\text{A7})$$

In the latter case, the inverse Compton is energetically not important, if

$$\frac{\gamma_c}{\gamma_m} \gg \left(\frac{10^{-2}}{\epsilon_B}\right)^{\frac{1}{p-2}}. \quad (\text{A8})$$

One can easily check, using the above criteria and Fig. 4, that for our specific model the inverse Compton process does not dominate electron cooling at any moment.

It should be noted, however, that the inverse Compton process can be imprinted in the afterglow light curves, even if the Compton cooling is less efficient than the synchrotron one. At the moment when the Compton component drifts down to the observed band, the light curve is expected to flatten. Chiang & Dermer (1999) demonstrated that this effect can be visible in the X-ray light curves; in the optics it appears very late and is already too weak to be observed, especially if overshadowed by the host galaxy.

FIGURE CAPTIONS

Fig. 1.— The bulk Lorentz factor of the blast wave as a function of a distance from the central engine. *Thin line*: for $\theta_j = \text{const} = \theta_{j0}$; *solid line*: for $\theta_j = \theta_{j0} + 1/\sqrt{3}\Gamma$; *dotted line*: for $\theta_j = \theta_{j0} + 1/\Gamma$. The numbers along the curves show the observed time as measured in seconds and given by Eq. (21).

Fig. 2.— The accretion rate as a function of a distance from the center, calculated for the same models as Fig. 1.

Fig. 3.— Evolution of the energy distribution of relativistic electrons. From the bottom to the top, the curves are for t : 1, 10, ..., 10^7 seconds.

Fig. 4.— The minimum injection electron energy, γ_m , and the “cooling” electron energy, γ_c , as a function of time.

Fig. 5.— The evolution of the apparent radiation spectra. The numbers mark the observed times.

Fig. 6.— The afterglow light curves: *the dotted lines* are the X-ray light curves and *the solid lines* are the optical light curves. The thick lines are for $\theta_{obs} = 0$ while the thin lines are for $\theta_{obs} = 0.28$.

Fig. 7.— The light curves in the time range, where the beaming effects are strongest. *The thin solid line* is for $\theta_j = \theta_{j0}$; *the thick solid line* is for $\theta_j = \theta_{j0} + 1/\sqrt{3}\Gamma$; *the dotted line* is for $\theta_j = \theta_{j0} + 1/\Gamma$; and *the dashed line* is for $\theta_j = \pi$ (spherical case).

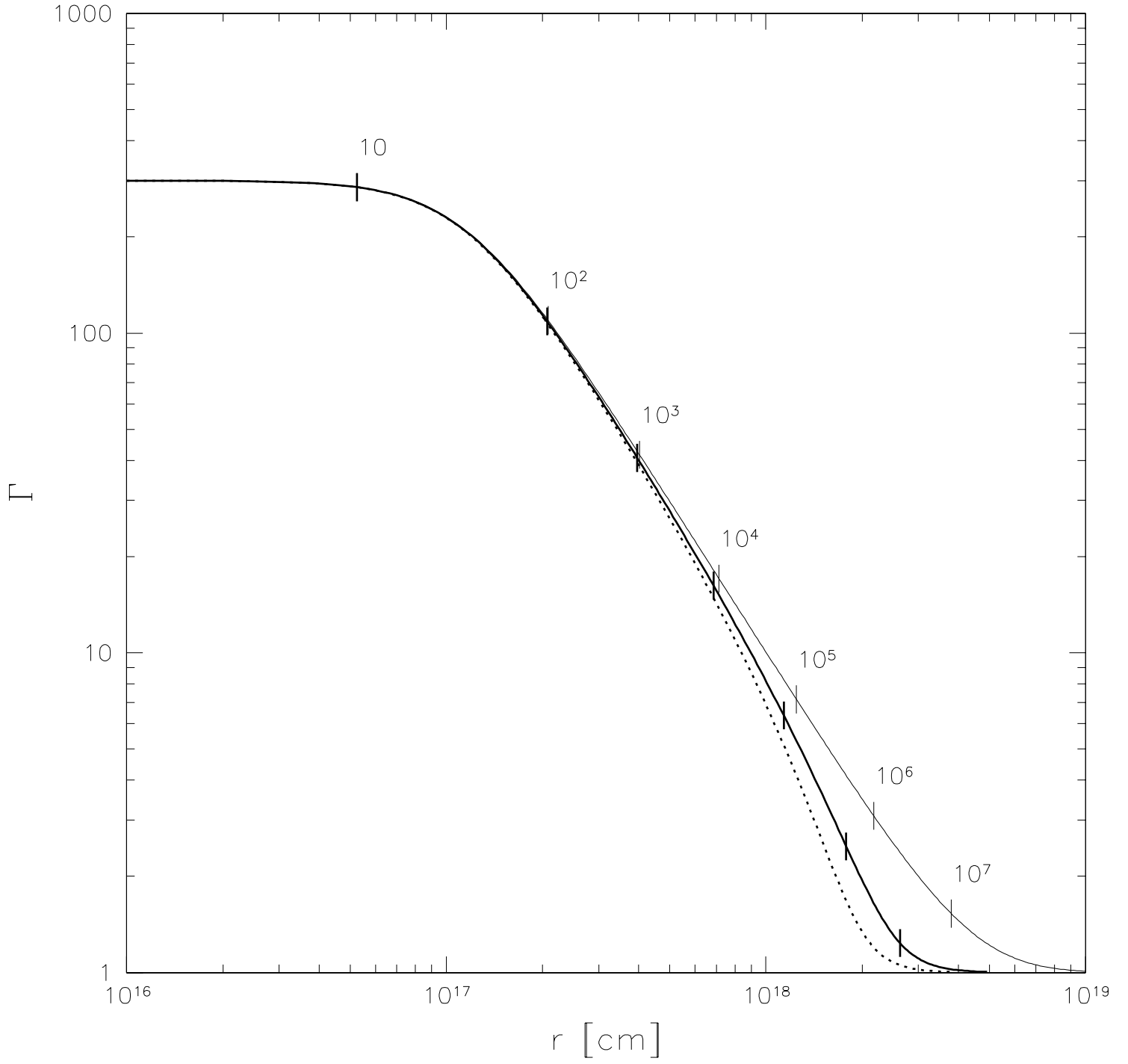


FIG 1.—

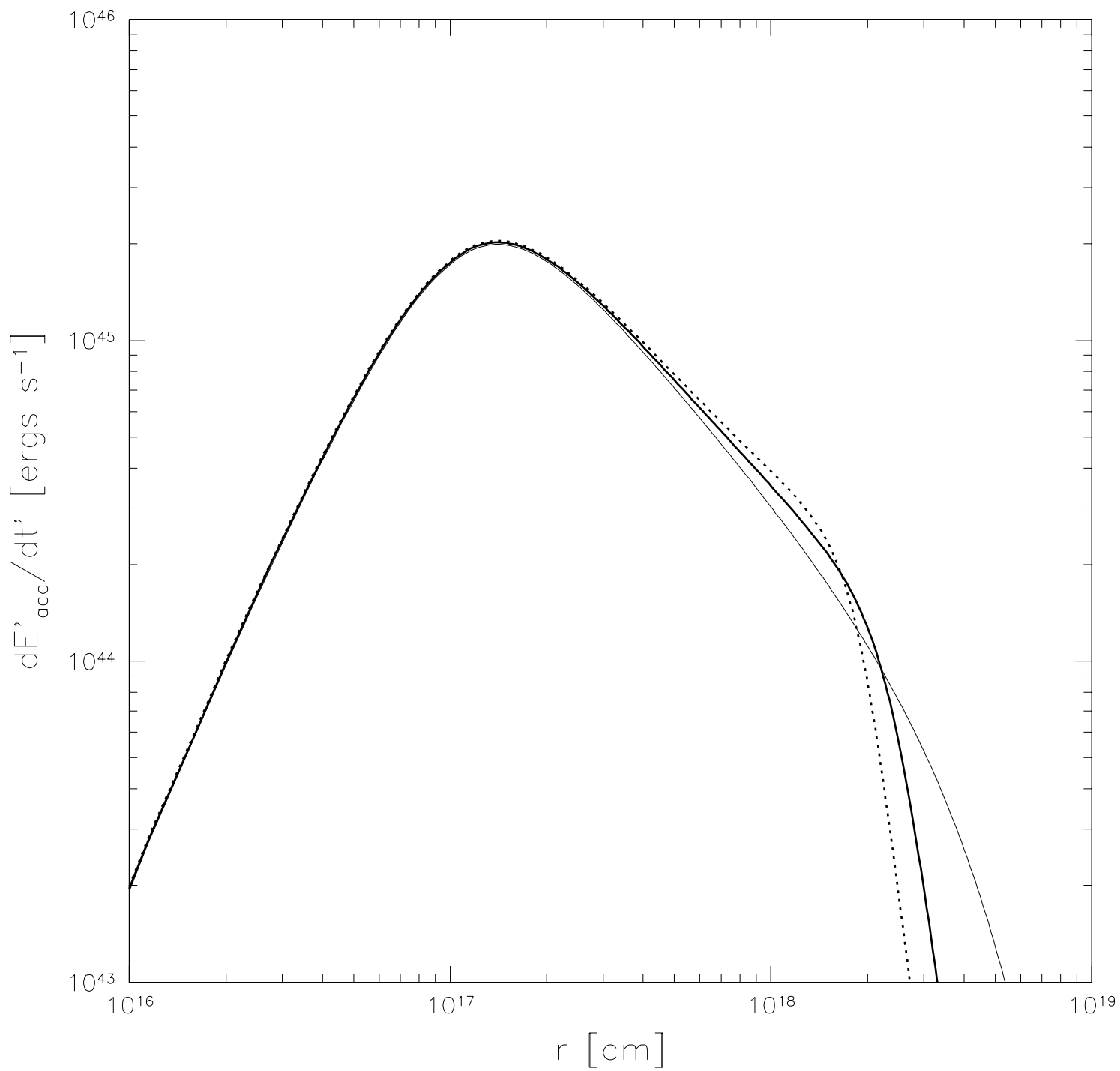


FIG 2.—

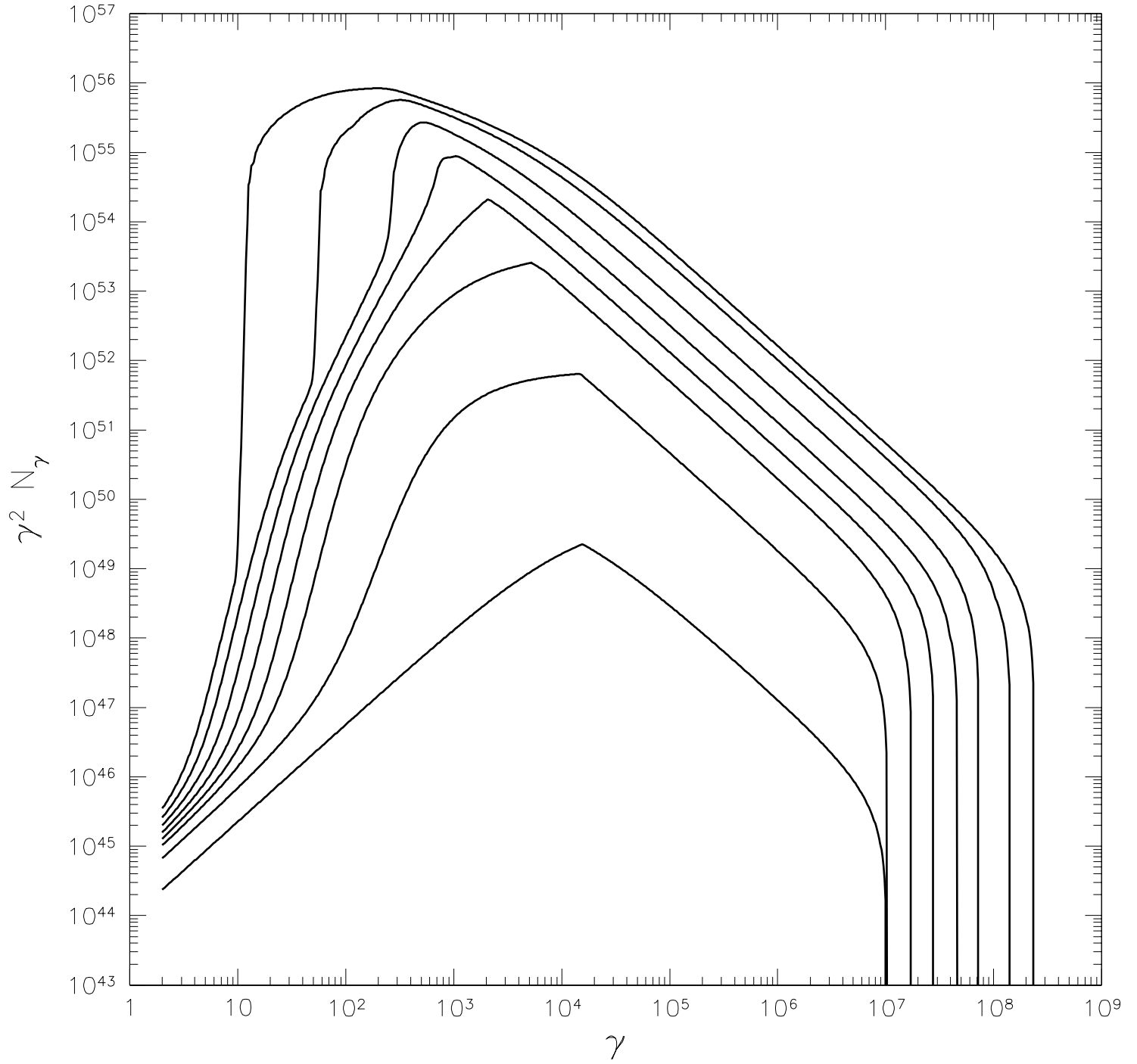


FIG 3.—

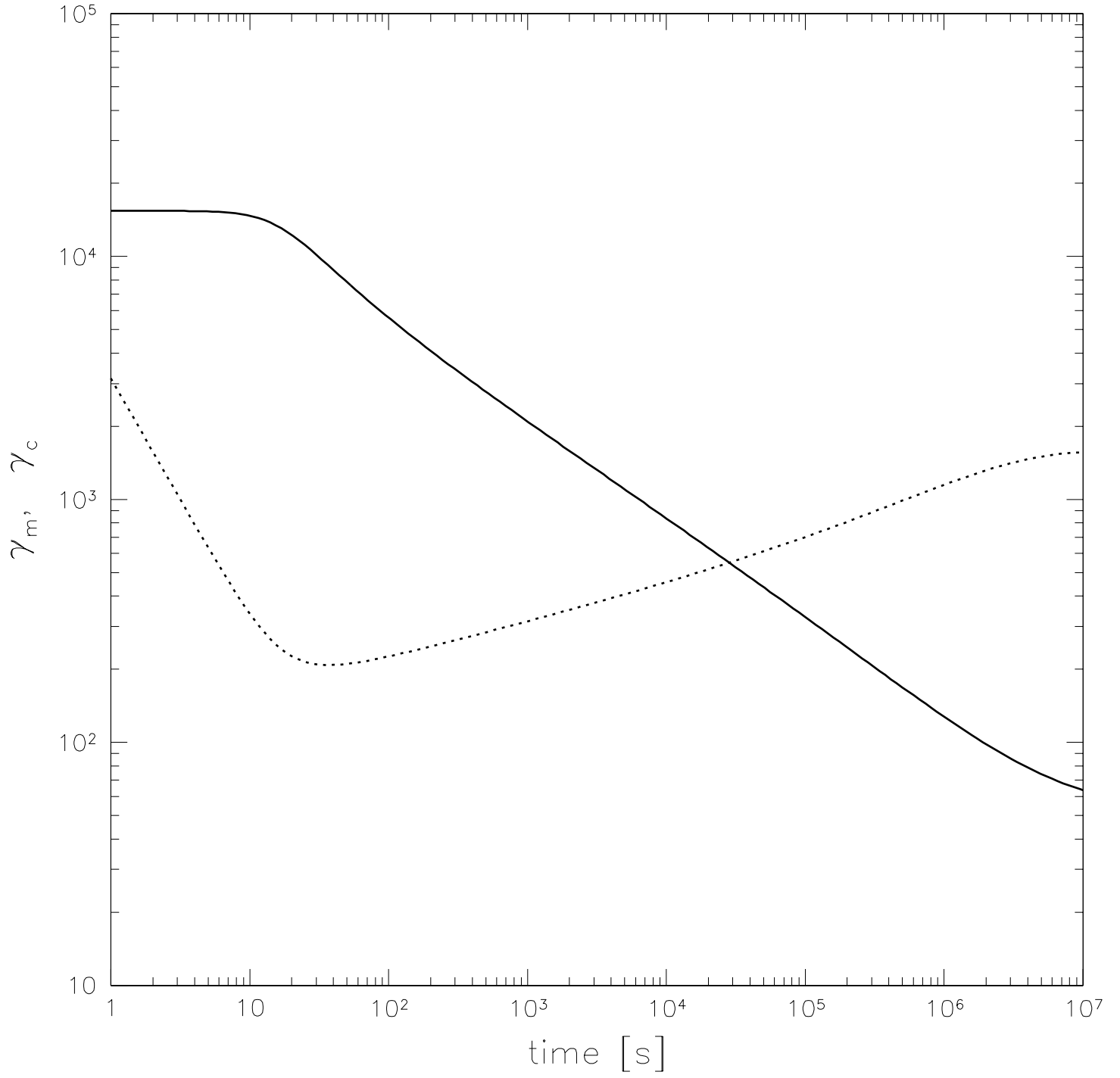


FIG 4.—

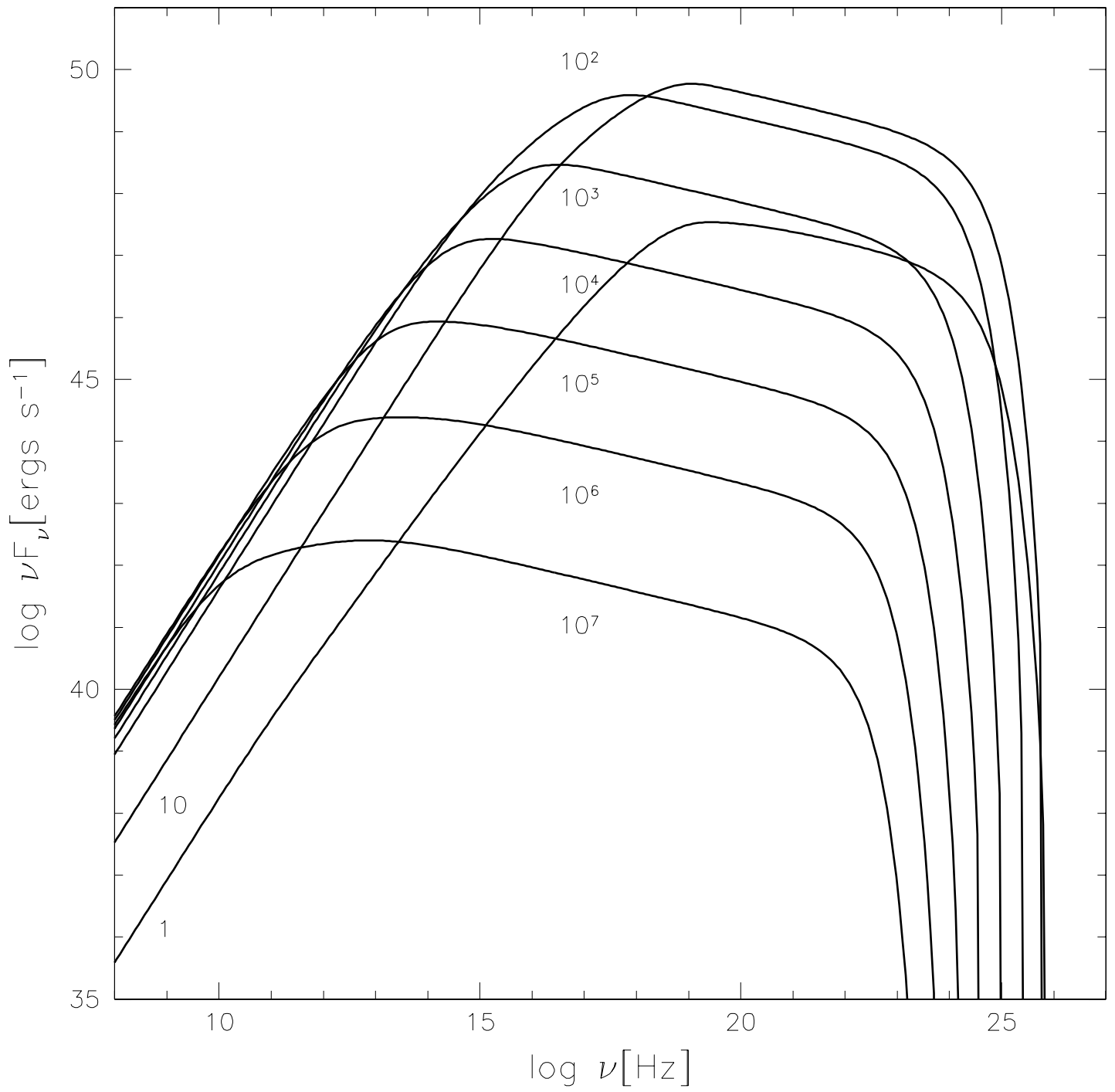


FIG 5.—

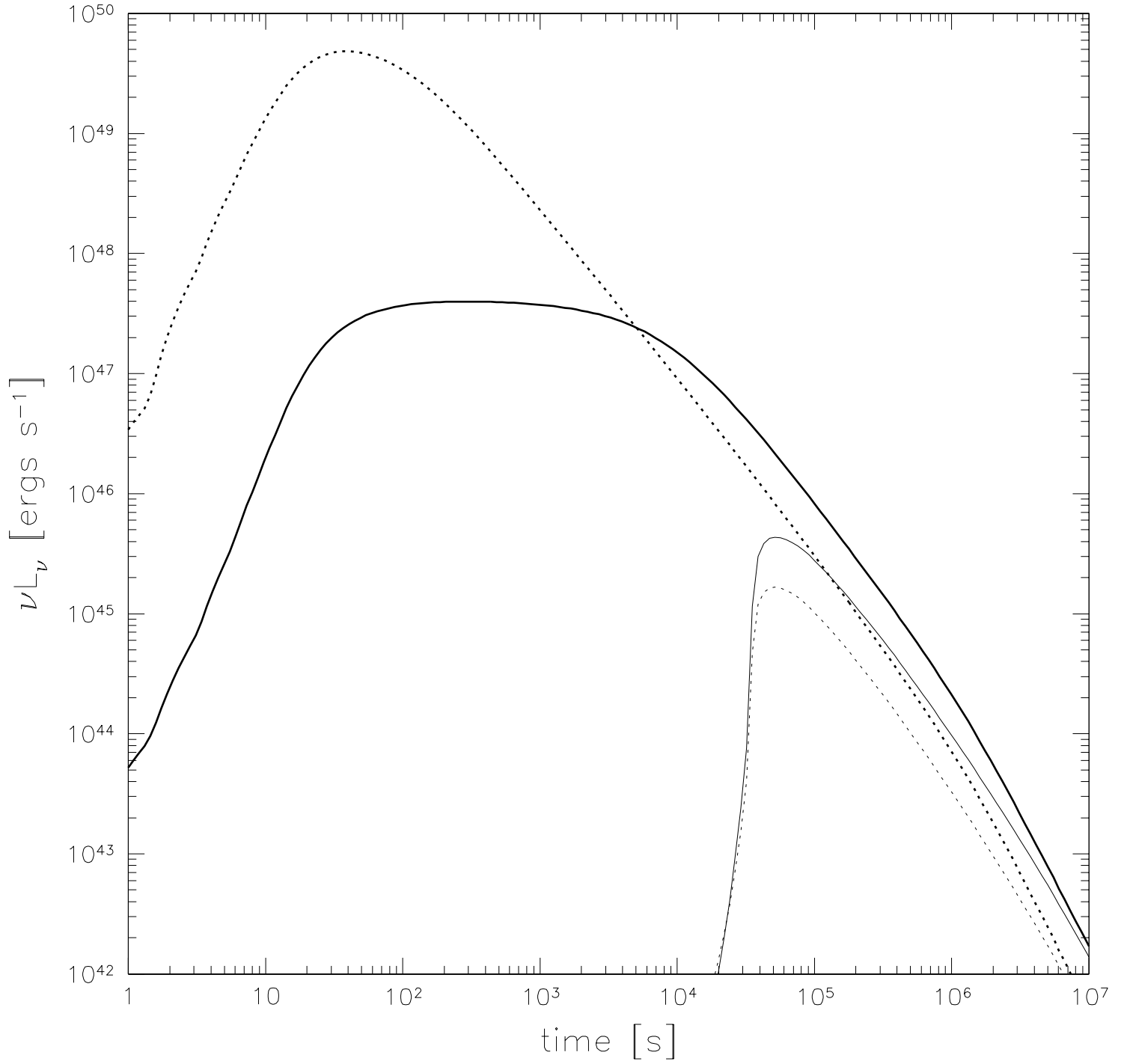


FIG 6.—

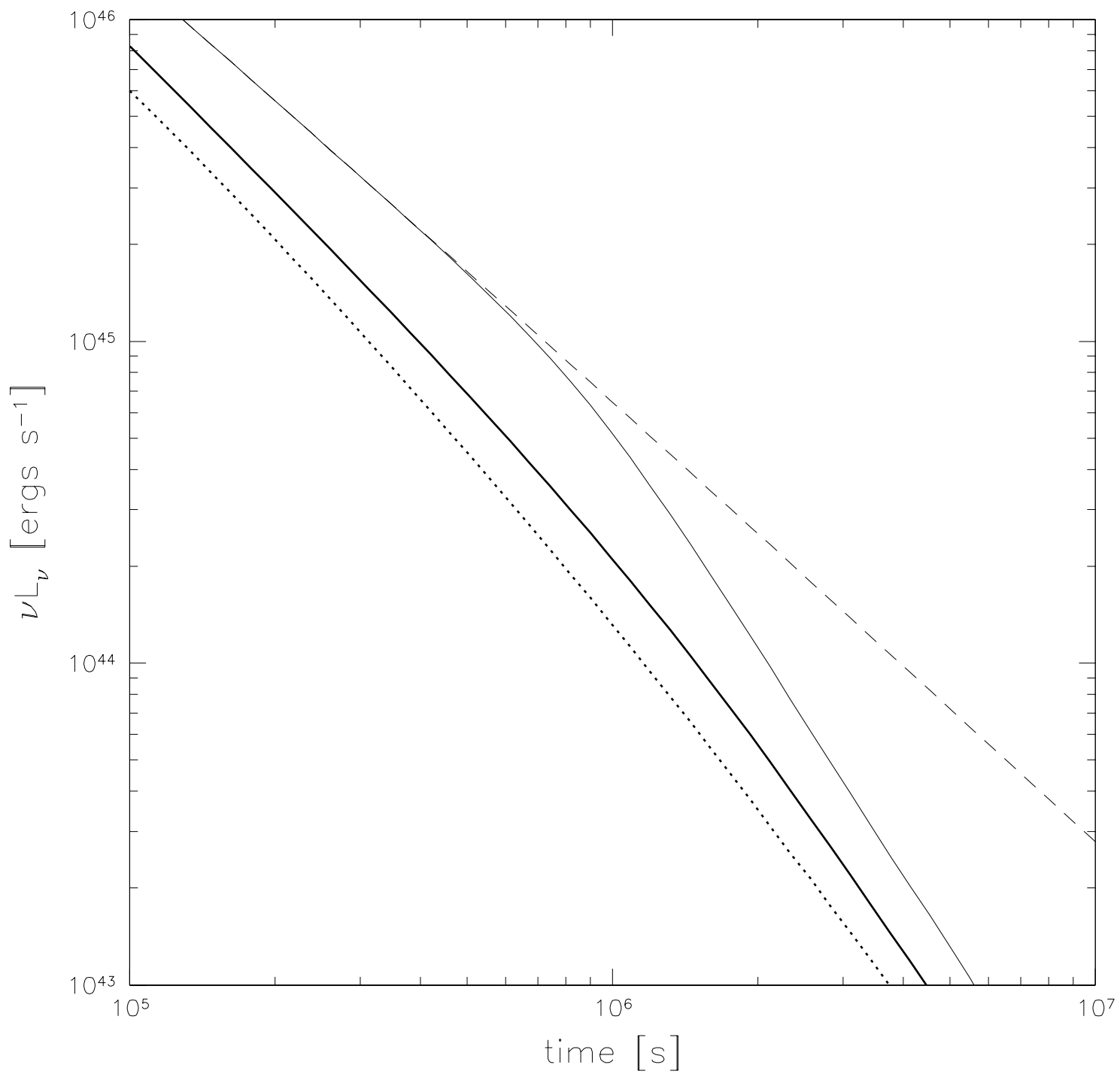


FIG 7.—